BALLISTIC IMPACT ON THIN SANDIWCH PANELS AND MULTI-LAYERED PLATES

D.W. ZHOU[1,]
TWI LTD, Cambridge, UK
dzhou@cantab.net

W.J. STRONGE[2]
Department of Engineering, University of Cambridge, Cambridge, UK

ABSTRACT

Ballistic perforations of monolithic steel sheets, two-layered sheets and lightweight sandwich panels were investigated both experimentally and numerically. The experiments were performed using a short cylindrical projectile with either a flat or hemispherical nose that struck the target plate at an angle of obliquity. A total of 170 tests were performed at angles of obliquity 0^0-45^0. The results suggest that during perforation by a flat nosed projectile, layered plates cause more energy loss than monolithic plates of the same material and total thickness. There was no significant difference in the measured ballistic limit speed between monolithic plates and layered plates during oblique impact perforation by a hemispherical nosed projectile.

To develop understanding of the process of fracture development and perforation of a thin stainless steel sheet resulting from oblique impact by a hard, flat-nosed projectile, numerical simulations by ABAQUS/Explicit finite element code were compared against residual velocities and ballistic limits of perforated plates. Effects of projectile length to diameter ratio for flat-nosed projectiles were investigated. For projectiles of equal mass, a longer projectile (larger ratio of length to diameter, $L/D > 2$) results in a drastic decrease in the ballistic limit speed for a double layered plate.

1. INTRODUCTION

For armour that protects against perforation by projectiles, there has been a long dispute over the benefits of replacing monolithic plates by multi-layered plates either with or without spacing [1-5]. A summary of the main conclusions of the Refs [1-5] is given in Table 1.

Although the sandwich plate is a variant of a multi-layered plate, there is still a considerable difference between a layered structure (with or without spacing) and sandwich construction. The distinctive structure of sandwich panels requires a special treatment for analyzing projectile impact problems. Goldsmith et al [6] conducted a series of tests on aluminium sandwich panels that were subjected to impact by various projectiles. The results showed that perforation of the panel was related principally to piercing of the facesheets. So far, most research on ballistic perforation of multi-layered plates and sandwich panel considered normal impact only. To the best of the present authors' knowledge, no experimental results were reported in the open literature about multi-layered targets under oblique impact.

The present paper gives a comparison of the ballistic impact resistance of stainless steel sheets, i.e. monolithic, double layered and sandwich sheets. In particular, effects of projectile nose shape, angle of obliquity on the ballistic resistance of layered plates and sandwich panels are addressed. In the following analysis, the ballistic limits of different types of plate are first experimentally determined. With an appropriate selection of

material constitutive relation and fracture criterion, the perforation sequence is numerically simulated. Effects of length to diameter ratio are discussed using the validated numerical analysis.

Table 1 Summary of ballistic impact on multi-layered plates

Reference	Proj. Mat.	Proj. nose shape[1]	Proj radius (mm)	Total thick (mm)	No. of layers	Impact speed(m/s)	Results*
Marom [1]	pure or alloy Al	round	2.8	1~10	1~3	350~ 390	$\Delta E^a < \Delta E^b$ $\Delta E^c < \Delta E^b$
Corran [2]	steel	flat	6.25	1.2~6.4	1	40~220	$\Delta E^a < \Delta E^b$
				2.4~6	2~3		
Radin [3]	2024-0 Al	flat conical	6.25	3.2	2	80~240	$V_{50}^a > V_{50}^b$
				4.8	3		
				6.4	4		
Gupta [4]	mild steel	ogive	3.1	4.7~25	1~6	800~ 870	$\Delta E^a > \Delta E^b$
	Al			6.1~40	1~6		
Almohandes [5]	steel, FRP	ogive	7.62	8	1 ~5	706~ 826	$\Delta E^a > \Delta E^b$ $\Delta E^c < \Delta E^b$

* All the results are for normal impact, ΔE is the decrease in kinetic energy of the projectile and V_{50} is the ballistic limit. Superscripts are defined as a=monolithic, b=layered no space, c=layered, spaced

2. EXPERIMENT DESCRIPTION

The experiment consisted of a cylindrical projectile with either flat or hemispherical nose shape that was fired from an air gun and struck a clamped circular plate at an angle of obliquity of either 0, 30 or 45 degrees. The angle of obliquity from normal α_i is described in Figure 1. To examine the effect on the ballistic limit of the projectile mass and the length to diameter ratio, four projectiles with the same diameter but different lengths were considered for each nose shape. Table 2 gives a complete list of the projectile parameters used in the experiment.

A nitrogen gun with a bore diameter 12.7 mm was used to accelerate the projectiles to a range of impact speeds from 50 ~ 150 m/s. The cylindrical projectiles have a diameter of 12.68 mm. The missile speed was roughly controlled by varying both the gas pressure in the high pressure cylinder that powers the gun and the location of the projectile in the barrel before firing. The muzzle speed was measured by a digital timer which measured the elapsed time between the breaking of two graphite leads that spanned the barrel at the muzzle; the distance between break-wires was 50 mm. The motion of the projectile was recorded by a high speed camera with a frame speed of either 4500 or 9000 fps; this was supplemented by a mirror to reflect the projectile movement. By analysing the frames recorded by the high speed camera, the residual

speed of the projectile can be measured. Using this measurement approach, an error of 10% is introduced in the residual speed due to the displacement measurement.

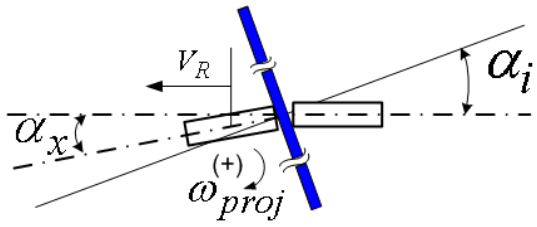

Figure 1 Schematic of oblique impact

Table 2 Projectile parameters used in the experiment

Name	Nose	Length (mm)	Length/Diameter	Mass (g)
F_1	Flat	18.7	1.5	20.5
F_1.5	Flat	28.1	2.2	30.8
F_2	Flat	37.4	2.9	41.0
F_2.5	Flat	46.8	3.7	51.3
H_1	Hemisphere	20.3	1.6	19.9
H_1.5	Hemisphere	30.5	2.4	29.9
H_2	Hemisphere	40.6	3.2	39.8
H_2.5	Hemisphere	50.8	4.0	49.8

To avoid the influence of the boundary, the diameter of the target plate was set to be about 12 times the diameter of the missile which had a diameter of 12.7 mm. The target plates of square shape have small holes near the edge and were bolted in a special designed mount; this resulted in a circular plate of 150 mm diameter with clamped boundary condition. After the tests, the holes in the plate had little elongation; this showed that the plate boundary was well clamped and had little radial movement. While these target plates may not be large enough to entirely eliminate effects of boundary clamping on the ballistic limit, numerical simulations indicate the influence of boundary effects is small.

The target plates consisted of 316L stainless steel sheets, including monolithic (0.5 mm thickness), double layered in contact (either 2x0.2 mm or 2x0.25 mm thickness) and sandwich sheets. The sandwich sheets, named HSSA, are thin, lightweight structures with stainless steel facesheets separated by a random arrangement of independent stainless steel fibres. Adhesive bonding is used to connect the facesheet and the core. The facesheet of the sandwich panel has a thickness of 0.2 mm and the fibrous core is 0.8 mm thick. A detailed mechanical modelling of this material is given in Ref. [7].

A total of 170 tests were carried out for these different targets. For a specific impact, the number of impact tests varied from 3-10 depending on whether the ballistic limit speed was determined quickly. However, there were around 20 tests for each impact when steel and HSSA sandwich panels were struck by relatively short projectiles, i.e., F_1, F_1.5, H_1 and H_1.5.

3. EXPERIMENT RESULTS

The resistance of structure to ballistic impact can be characterized by the ballistic limit and energy absorption during perforation. The ballistic limit of a plate impacted by a particular projectile is taken as the average of the lowest speed giving a complete perforation and the highest speed that gives partial or no perforation. In some cases where the target plates were cracked, the corresponding projectile incident speed was taken as the ballistic limit speed because they are the best available estimate. Figure 3 gives a comparison of the ballistic limit of different layered plates as a function of angle of obliquity for a flat-nosed projectile (F_1). For a stainless steel plate struck at normal obliquity by a flat-nosed projectile, Figure 2 shows that the ballistic limit speed of the monolithic panel is largest while the ballistic limit speed of the sandwich panel is smaller. Double layered sheet (either 2 x 0.25 mm or 2 x 0.2 mm) has a ballistic limit between that of monolithic steel sheet and sandwich plate. However, for a flat-nosed projectile at an impact obliquity of 30^0, the double layered sheet clearly has a larger ballistic limit than a monolithic plate. Both the 2 x 0.25 mm double layered plate and 2 x 0.2 mm double layered plate have ballistic limits 17% and 12% larger than the monolithic sheet, respectively. This observation demonstrates that for oblique impact of thin stainless steel plates by flat-nosed projectiles at angle of obliquity smaller than 45^0, double layered structures are more effective in resisting projectile perforation than monolithic plates of the same total material thickness. A comparison of the ballistic limits of sandwich panels and monolithic sheets also supports this conclusion. As seen in Figure 2, for both flat and hemispherical nosed projectiles, the ballistic limit of monolithic sheets is 23% larger than that of HSSA sandwich sheets at normal obliquity. This percentage decreases to 13% for an angle of obliquity 30^0 and 7% for 45^0.

Residual velocities of various projectiles for monolithic plates and HSSA sandwich panels are given in Figure 3. A curve of best fit to the experiment data is also given. The empirical formula employed in the best fit curve is from Ref. [8]

$$V_R = \begin{cases} 0 & 0 \le V_i \le V_{50} \\ p_1 (V_i^{p_2} - V_{50}^{p_2})^{1/p_2} & V_i \ge V_{50} \end{cases} \quad (1)$$

where V_i, V_R and V_{50} are the striking, residual and ballistic limit velocities of the projectiles (in m/s). For nondeforming projectiles, $p_2 = 2$ and $p_1 = \dfrac{M_1}{M_1 + M'/3}$

where M_1 is the projectile mass and M' is the target material enclosed within a projection of the projectile prior to impact. Equation (1) is obtained from conservation of energy for plugging where plug mass is $M'/3$ and energy required for perforation is independent of impact speed.

4. NUMERICAL SIMULATION

4.1 General description

In order to understand the perforation process, ABAQUS/Explicit was employed to simulate both monolithic plates and layered plates under projectile impact. A numerical simulation of oblique impact requires a 3D model of the plate deformation. Since membrane stretching is a main mechanism of energy absorption, 4 node shell elements (S4R) with reduced integration were used. Both the plate and the projectile are

symmetrical. Consequently, only half of the plate with a symmetric boundary along a diameter was considered. A typical element size of 0.2 mm was used near the perforated area.

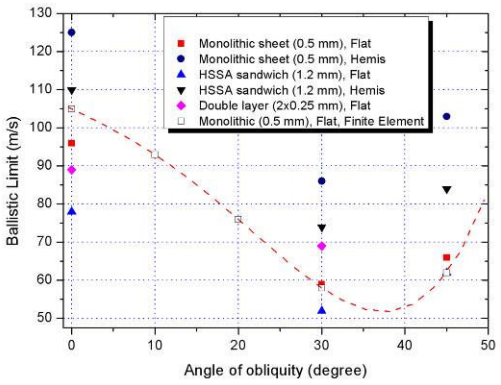

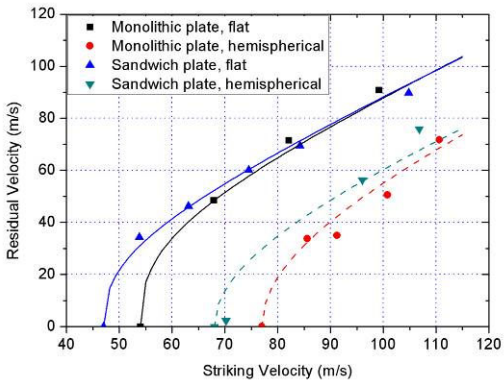

Figure 2 Figure 3

Figure 2 Ballistic limits of structures struck by flat and hemispherical nosed cylinders (F_1, H_1) compared with finite element simulation

Figure 3 Measured residual speed curves for different plates struck by different projectiles (F_1.5, H_1.5) at angle of obliquity 30 degree

The numerical model employed a uniform thickness plate with clamped edge that represents the boundary condition in this experiment. The ABAQUS/Explicit general contact algorithm was employed to simulate the contact between the projectile and plate. This contact algorithm was also used to simulate the interaction of the two faceplates in a double layered plate. During the perforation, the petal, that develops, bends until it comes into contact with the non-perforated area of the plate. The self contact algorithm was used to consider this interaction. Friction is neglected in the simulation since sensitivity studies show that the result was not sensitive to the friction coefficient. The experiments employed a hardened projectile which had no observable plastic deformation after perforating the plate; consequently the projectile was modelled as an elastic body. The projectile had a Young's modulus 210 GPa and Poisson ratio of 0.3. Densities of the projectile and plate were taken as 7800 kg/m^3.

Johnson-Cook material model was used in the present simulation to simulate the sandwich facesheets and single/layered panels. This empirical model decouples the effect of strain, strain rate and temperature, namely,

$$\sigma = [A + B\bar{\varepsilon}^n][1 + C\ln(\frac{\dot{\varepsilon}}{\dot{\varepsilon}_0})][1 - \hat{\theta}^m] \qquad (2)$$

where σ is the flow stress; $\bar{\varepsilon}$ is the equivalent plastic strain; C and $\dot{\varepsilon}_0$ are material properties measured at transition temperature. Parameters A, B, and n are determined from the uniaxial tension test in last section. Parameter $\hat{\theta}$ represents the adiabatic heating and this effect is ignored in the analysis.

It has been shown that localization of the deformation and strain-softening behaviour of the material cause mesh dependence in simulation of continuum damage mechanics. Mesh refinement results in a smaller width of the localization band and reduces the global energy dissipation. The damage thus localizes in a zone of vanishing volume and consequently the energy dissipation decreases to physically unrealistic values. However, Needleman [9] has shown that pathological mesh dependence does not occur in numerical simulation for rate dependent solids because material rate dependence implicitly introduces a length scale into the governing equations.

The basic form of a strain based fracture model in FE analysis is to define the damage in an element

$$\omega_D = \int \frac{d\bar{\varepsilon}}{\bar{\varepsilon}_f} \tag{3}$$

where $\bar{\varepsilon}_f$ is the equivalent plastic strain to fracture and $d\bar{\varepsilon}$ is an increment of equivalent plastic strain. The state variable ω_D increases monotonically with plastic deformation proportional to the incremental change in equivalent plastic strain. Fracture is assumed to occur when $\omega_D = 1.0$.

The equivalent fracture strain $\bar{\varepsilon}_f(\sigma_m/\bar{\sigma})$ to be used in FE analysis strongly depends on stress triaxiality $\frac{\sigma_m}{\bar{\sigma}}$ where σ_m is the hydrostatic or mean stress and $\bar{\sigma}$ is the VonMises equivalent stress. The fracture strain at other stress triaxiality can be obtained by

$$\bar{\varepsilon}_f = \frac{D_c}{\sigma_m/\bar{\sigma}} \tag{4}$$

where D_c is a critical damage value for a material, which can be obtained through an uniaxial tension test. For the uniaxial tension test, stress triaxiality is taken as 0.33 since the material has very small thickness. Thus, the damage value D_c is approximated as

$$D_c = \frac{1}{3}\bar{\varepsilon}_f(\sigma_m/\bar{\sigma}) \tag{5}$$

The sandwich panels used in these tests had a core consisting of randomly oriented stainless steel fibres. The fibrous core of the sandwich panel can be represented as a compressive anisotropic plastic material. The present simulation employed a material model similar to that developed by Xue and Hutchinson [10]. ABAQUS subroutine VUMAT has been implemented to simulate the plastic deformation and core failure. Fracture of the fibrous core is simulated by deleting elements once the strain fracture criterion is satisfied. Because simulation results suggest that the kinetic energy of the projectile is predominately absorbed by stretching of the facesheets, the effect of the fibrous core in sandwich panel is solely to provide spacing between the two facesheets.

4.2 Determination of facesheet and panel material properties

The uniaxial tensile test was performed to identify the material properties to be used in the numerical simulation. Flat, dog-bone specimens were cut from thin sheets. Two types of panel material were investigated, i.e., HSSA sandwich panels (1.2 mm total

thickness) and 316L stainless steel sheets (0.5 mm thickness). This thickness gives the same areal density between sandwich panels and monolithic plates. An Instron machine was employed to exert the tensile loading (at strain rate of 0.001 s^{-1}) until the specimen was fractured. The elongation of the specimen was recorded by a laser extensometer.

The true stress-strain curve was obtained by numerical simulation with a trial-and-error approach until the numerical calculation of the load and necking deformation corresponded well with the test data on the test specimen. Numerical simulation of the tensile test was performed by ABAQUS/Explicit due to the instability problem in the implicit method when representing ductile fracture. The monolithic stainless steel specimen was meshed by plane stress elements. In the case of the HSSA sandwich panel, only two facesheets with thicknesses 0.2 mm each were incorporated in the FE model since the core has a negligible stretching stiffness. Relevant parameters (*A, B, n* in equation (3)) obtained from tensile test simulation were given in Table 3. By comparing the measured displacement at fracture of the specimen with the calculated displacement and evaluating the corresponding finite strain in the region of necking, we also obtained an estimate for the experimental fracture strain (see Table 3). The parameter C in equation (3) for the strain rate effect (Table 3) is determined by Nordberg [11]. On the basis of a comparison of 12 high strain rate tests of stainless steel, Nordberg suggested an empirical formula for the material constitutive relation of stainless steel. This formula is similar as equation (3) except that the thermal effect is ignored.

Table 3 Summary of material properties

Specimen	A (MPa)	B(MPa)	C	$\dot{\varepsilon}_0 (s^{-1})$	n	m	$\bar{\varepsilon}_f$
Monolithic plate	270	1250	0.07	0.001	0.72	0	0.46
HSSA facesheet	270	1250	0.07	0.001	0.73	0	0.32

4.3 Validation of numerical model

Figure 4 gives a comparison of residual velocities between experiment and FE analysis for target plates struck at angle of obliquity of 30^o. The FE analysis is in general within 20% of the experiment. For the ballistic limit, it has been shown that the calculated ballistic limit speed is within 10% of the experimental results.

5. DISCUSSION

5.1 Effect of projectile nose shape

The experimental results in the previous section show that for flat-nosed projectiles, a double layered plate has more impact resistance than a monolithic plate of the same material thickness in terms of both ballistic limit and speed drop. To develop understanding of the observed behaviour, the validated numerical model was employed to investigate the impact force during perforation. During plate perforation, a nose force acts on the projectile nose where it initially contacts the plate. After the plate is perforated and the projectile is passing through the plate it is subjected to a side force where it moves against the plate. During perforation, the nose and side forces cause the projectile to rotate and thus affect the ballistic limit speed.

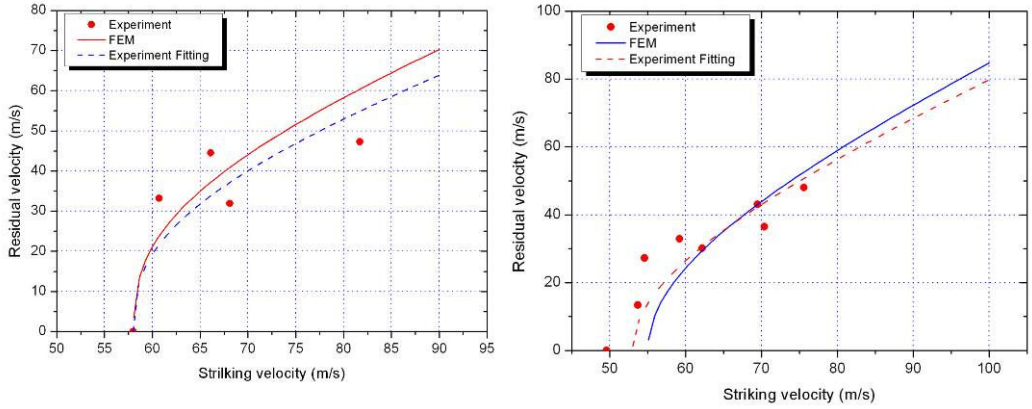

(a) 0.5 mm monolithic steel plate (b) HSSA sandwich sheet

Figure 4 Variation of residual speed with striking speed for a flat nosed projectile (F_1) striking on monolithic steel plates and HSSA sandwich panels at 30^0 angle of obliquity

Figure 5 illustrates the impact force during perforation of two types of plates (monolithic and double layered plates in contact) by a flat nosed projectile travelling at a moderately large impact speed (40% larger than the ballistic limit speed) and striking at a 30^0 angle of obliquity. It shows that the impact force generated by a double layered plate is much larger than that by a monolithic plate. An observation of the deformation of the double layered plate (without space) from FE analysis indicated that individual plates do not fail simultaneously; this asynchrony increases the penetration resistance because, when the first plate is perforated, the second faceplate is stretched without fracture initiation. This stretching causes strain hardening and thus the resistance of the second plate to perforation is increased. These effects hence lead to a larger average impact force than that for a monolithic plate.

With increasing impact speed, the impact duration in both cases becomes shorter and the effect of the asynchrony in fracture in layered plates becomes insignificant. Therefore, the nose force for both monolithic and layered plates of equal material thickness will be identical; the difference in energy loss in perforation of these two structures will thus be negligible.

When a projectile with a hemispherical nose shape strikes a plate, the numerical simulation shows that the difference in the impact force between monolithic and layered sheets is insignificant (maximum 10% difference). This similarity indicates that these two structures will have similar impact resistance, giving negligible difference of the residual speed and ballistic limit between a monolithic plate and a double layered plate.

5.2 Effect of projectile length to diameter ratio for oblique perforation

The present section investigates the effect of the projectile length/diameter ratio on the ballistic impact of plates of the same mass. The length/diameter ratio can affect perforation because of increasing moment of inertia about a transverse axis and decreasing mass per unit cross-sectional area as projectile length increases. Figure 6 gives a comparison of residual speed of a flat nosed projectile for two length/diameter ratios, i.e., L/D =1.64 and 4.67. For both monolithic and layered sheets, it can be seen that the ballistic limit decreases rapidly with increasing length/diameter ratio. However,

with increases of the striking speed, the effect of the length/diameter becomes insignificant. This might be because the influence of projectile rotation about a transverse axis is smaller for a higher striking speed since the impact event is so short.

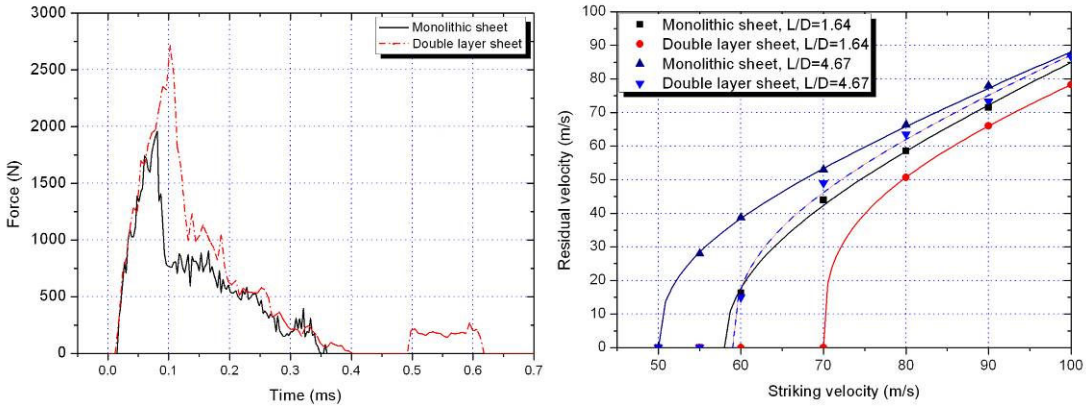

Figure 5 Calculated force on the flat nosed projectile (F_1, *L/D* =1.64) during perforation of monolithic and layered sheets at an impact speed 80 m/s and an initial angle of obliquity of 30 degree

Figure 6 Calculated residual speed of a monolithic plate and double layered sheet in contact struck by flat nosed projectiles with L/D=1.64 and 4.67 at angle of obliquity of 30 degree.

6. CONCLUSIONS

This experimental study compared the ballistic resistance of monolithic plates, double layered sheets and sandwich panels. The main findings are summarized below.

(i) At angles of obliquity 0^0-45^0, a flat nosed projectile has a smaller ballistic limit than a hemispherical projectile as a consequence of more localized deformation near the penetrating corner of the projectile nose.
(ii) For oblique impact by a flat-nosed projectile at angles of obliquity 0^0-45^0, layered plates have a larger ballistic limit than monolithic plates composed of the same material and having the same total material thickness.
(iii) For oblique impact by hemispherical-nosed projectiles, monolithic plates and sandwich panels have nearly the same ballistic limit speed.

FE simulations of oblique impact of cylindrical projectiles on thin panels (monolithic steel plate or double layered sheet) generally resulted in a ballistic limit speed within 20% of experimental results. Achievement of this accuracy required refinement of material constitutive relations (including failure criterion across a range of projectile nose shapes and target configurations) and incorporation of strain-rate dependence.

This validated numerical model was used to investigate the energy loss in perforation of thin monolithic and layered plates struck at angles of obliquity 0^0-45^0 by flat and hemispherical nosed projectiles. For a flat nosed projectile, it was found that the ballistic resistance for layered sheets is much larger than that of a monolithic sheet. A

large length/ diameter ratio of the projectile causes a decrease in the ballistic limit of both monolithic and layered metallic sheets because inertia limits rotation of the projectile (pitch) that develops during perforation. The effect of L/D on the ballistic limit speed decreases however with increasing impact speed above the ballistic limit.

Reference

[1] I. Marom and S. R. Bodner, "Projectile perforation of multi-layered beams," *International Journal of Mechanical Sciences*, vol. 21, pp. 489-504, 1979.

[2] R. S. J. Corran, P. J. Shadbolt, and C. Ruiz, "Impact loading of plates -- An experimental investigation," *International Journal of Impact Engineering*, vol. 1, pp. 3-22, 1983.

[3] J. Radin and W. Goldsmith, "Normal projectile penetration and perforation of layered targets," *International Journal of Impact Engineering*, vol. 7, pp. 229-259, 1988.

[4] N. K. Gupta and V. Madhu, "An experimental study of normal and oblique impact of hard-core projectile on single and layered plates," *International Journal of Impact Engineering*, vol. 19, pp. 395-414, 1997.

[5] A. A. Almohandes, M. S. Abdel-Kader, and A. M. Eleiche, "Experimental investigation of the ballistic resistance of steel-fiberglass reinforced polyester laminated plates," *Composites Part B: Engineering*, vol. 27, pp. 447-458, 1996.

[6] W. Goldsmith, G.-T. Wang, K. Li, and D. Crane, "Perforation of cellular sandwich plates," *International Journal of Impact Engineering*, vol. 19, pp. 361-379, 1997.

[7] D. W. Zhou and W. J. Stronge, "Mechanical properties of fibrous core sandwich panels," *International Journal of Mechanical Sciences*, vol. 47, pp. 775-798, 2005.

[8] J. A. Zukas, T. Nicholas, H. F. Swift, L. B. Greszczuk, and D. R. Curran, *Impact dynamics*. New York: John Wiley & Sons, 1982.

[9] A. Needleman, "Material Rate Dependence and Mesh Sensitivity in Localization Problems," *Computer Methods in Applied Mechanics and Engineering*, vol. 67, pp. 69-85, 1988.

[10] Z. Xue and J. W. Hutchinson, "Constitutive model for quasi-static deformation of metallic sandwich cores," *International Journal for Numerical Methods in Engineering*, vol. 61, pp. 2205-2238, 2004.

[11] H. Nordberg, "Note on the sensitivity of stainless steels to strain rate," AvestaPolarit Research Foundation and Sheffield Hallam University, Report No. 04.0-1, 2004.